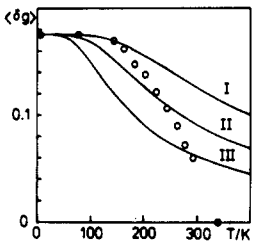

Figure 8. Temperature dependence of experimental and calculated $\langle \delta g \rangle$ values (eq 6), with ΔE = 200, 300, and 450 cm^{-1} (see text).

(Figure 8) clearly demonstrate that the applied model is only a very crude approximation. A more sophisticated theory would have to take into account explicitly the vibronic levels within the ground-state potential surface[34] and the fast relaxation between them, which leads to an averaging of the molecular g values and the Cu-N bond lengths at much lower temperatures than predicted by our simple model. Independent of a specific model, however, eq 4 and 6 allow us to correlate the extent of the Jahn-Teller distortion with the observed g values:

$$\frac{\langle \delta a \rangle}{\delta a} = \frac{\langle \delta g \rangle}{\delta g} \tag{8}$$

Thus the EPR investigations in dependence on temperature gave valuable information about the dynamic averaging process within the CuN_6 polyhedra, though complications due to exchange coupling effects occurred, and extended the results of the X-ray determinations at 298 and 110 K. Bonding parameters for the overlap between the metal $d_{x^2-y^2}$ orbital and the corresponding nitrogen s and p orbitals were also reported.

Acknowledgment. We thank the Fonds der Chemischen Industrie and the Deutsche Forschungsgemeinschaft for financial support. We thank Professor W. J. A. Maaskant (State University of Leiden) for helpful discussions. J.W. thanks the Netherlands Organisation for the Advancement of Pure Research (ZWO) for financial support.

Registry No. $[Cu([9]aneN_3)_2][Cu(CN)_3]\cdot 2H_2O$, 102920-57-0.

Supplementary Material Available: Tables of atom positional and anisotropic thermal parameters, bond distances and angles, and intraligand distances at 110 and 293 K (9 pages). Ordering information is given on any current masthead page.

(34) Riley, M. J.; Hitchman, M. A.; Reinen, D. *J. Chem. Phys.*, in press.

Contribution from the Departments of Chemistry and Physics, Faculty of Science, Kyushu University, Hakozaki, Higashiku, Fukuoka 812, Japan

Crystal Structure, Mössbauer Spectra, and Magnetic Properties of $[Fe(acpa)_2]PF_6$ and Crystallographic Changes in Fast Electronic Relaxation between $S = {}^1/_2$ and $S = {}^5/_2$

Yonezo Maeda,*† Hiroki Oshio,†§ Yoshimasa Takashima,† Masahiro Mikuriya,† and Masanori Hidaka‡

Received October 28, 1985

The crystal structure of the iron(III) complex $[Fe(acpa)_2]PF_6$ (Hacpa = *N*-(1-acetyl-2-propylidene)(2-pyridylmethyl)amine), which shows fast electronic relaxation between $S = {}^1/_2$ ($^2T_{2g}$) and $S = {}^5/_2$ ($^6A_{1g}$) with a spin-interconversion rate of about (2-3) × 10^6 s^{-1}, was determined. The crystal data for high-spin $[Fe(acpa)_2]PF_6$ ($FePF_6O_2N_4C_{22}H_{26}$) are as follows: monoclinic system, space group $P2/a$, a = 13.674 (1) Å, b = 9.911 (1) Å, c = 10.325 (1) Å, α = 90.00°, β = 110.43 (1)°, γ = 90.00°, V = 1311.3 (0) $Å^3$, R_w = 5.85%, d_{calcd} = 1.472, d_{found} = 1.46, Z = 2. The average bond distances, Fe-N = 2.117 Å and Fe-O = 1.939 Å, are in good agreement with the corresponding values reported for high-spin isomers of other spin-crossover iron(III) complexes. The temperature profiles of the integral intensities of (0n0) reflections derived from energy-dispersive X-ray diffraction were observed in the vicinity of the spin-transition temperature and showed a continuous variation with temperature which parallels that of the high-spin fraction. The results are interpreted in terms of a model in which the spin interconversions are accompanied by continuous atomic displacements within the same lattice and treated as an intramolecular mechanism.

Introduction

A number of spin-crossover iron complexes have so far been reported.[1-5] Recently iron(III) compounds that flip spin at a rate faster than the ^{57}Fe Mössbauer lifetime (1×10^{-7} s) have been reported.[6-11] A smooth increase of magnetic moments with increasing temperature is observed for complexes of this type, and those Mössbauer spectra show relaxation phenomena in the transition region. The magnetic property of the spin-crossover complex $[Fe(acpa)_2]PF_6$, which shows a spin-interconversion rate as fast as the Mössbauer lifetime of the excited state of ^{57}Fe, has been reported very recently.[6]

In the present experiment, energy-dispersive X-ray diffraction (EDD) was carried out to study structural transitions and/or the microstructural changes in the vicinity of a spin transition for this complex. It is important to observe a wide region of the wave vector Q (=$(4\pi \sin\theta)/\lambda$) to obtain microstructural information. The EDD method may be correlated to the usual angular-dispersive X-ray diffraction (ADD) by the following relations. In the EDD method, the Bragg condition is $2d_j \sin\theta = \lambda_j = 12.4/E_j$ (E in keV), on the other hand, $2d_j \sin\theta_j = \lambda$ in the ADD method. In the EDD method, experiments are done at fixed scattering angles and variable energy. The easy change in energy, E_j, is useful for selecting the energy of reflection outside the absorption edge of the constituent atoms in the specimen used. The EDD method is characterized by observing more reliable reflection

† Department of Chemistry.
‡ Department of Physics.
§ Present address: Institute for Molecular Science, Okazaki, Aichi 444, Japan.

(1) Ewalt, A. H.; Martin, R. L.; Sinn, E.; White, A. H. *Inorg. Chem.* **1969**, *8*, 1837.
(2) König, E.; Ritter, G.; Irler, W.; Goodwin, H. A. *J. Am. Chem. Soc.* **1980**, *102*, 4681.
(3) Rickards, R.; Johnson, C. E.; Hill, H. A. O. *J. Chem. Phys.* **1968**, *48*, 5231.
(4) Epstein, L. M.; Straub, D. K. *Inorg. Chem.* **1969**, *8*, 784.
(5) Hoselton, M. A.; Wilson, L. J.; Drago, R. S. *J. Am. Chem. Soc.* **1975**, *97*, 1722.
(6) Maeda, Y.; Tsutsumi, N.; Takashima, Y. *Inorg. Chem.* **1984**, *23*, 2440.
(7) Ohshio, H.; Maeda, Y.; Takashima, Y. *Inorg. Chem.* **1983**, *22*, 2684.
(8) Federer, W. D.; Hendrickson, D. N. *Inorg. Chem.* **1984**, *23*, 3861, 3870.
(9) Kunze, K. R.; Perry, D. L.; Wilson, L. J. *Inorg. Chem.* **1977**, *16*, 594.
(10) Hall, G. R.; Hendrickson, D. N. *Inorg. Chem.* **1976**, *15*, 607.
(11) Timken, M. D.; Hendrickson, D. N.; Sinn, E. *Inorg. Chem.* **1985**, *24*, 3947.

0020-1669/86/1325-2958$01.50/0

intensities than the ADD method and has been developed by Hidaka et al.[12]

Experimental Section

The Hacpa ligand was prepared by adding 2-(aminomethyl)pyridine (2.16 g, 20 mmol) in 20 mL of methanol to a solution of acetylacetone (2.00 g, 20 mmol) in 20 mL of methanol. Then, the solution was refluxed until it turned yellow. Triethylamine (2.02 g, 20 mmol) dissolved in 20 mL of methanol was added to this solution, and the solution was stirred for an additional 15 min. To this solution was slowly added $Fe(NO_3)_3 \cdot 9H_2O$ (4.04 g, 10 mmol) dissolved in 20 mL of methanol. After 1 min, NH_4PF_6 (3.2 g, 20 mmol) in 20 mL of methanol was added and the solution was warmed for 5 min and then cooled. The solution was permitted to stand overnight. The crude product of blue-black solid was collected by filtration and washed with methanol. The crude product was recrystallized from dichloromethane. The ^{57}Fe-enriched complexes were prepared by the same method as that mentioned above, using ^{57}Fe-enriched $Fe(NO_3)_3 \cdot 9H_2O$ that was prepared from $^{57}Fe_2O_3$. Single crystals of the complexes were obtained by slow evaporation of dichloromethane at room temperature. The solid samples crsytallized in the same preparative vessel were used for all measurements examined in this study except the Mössbauer measurements for ^{57}Fe-enriched samples.

Magnetic susceptibility data on the polycrystalline samples at various temperatures (78–304 K) were obtained by the Faraday method, using an electrobalance, Type 2002 (Cahn Instrument) with an electromagnet of 8000 G. The temperature was controlled over 78–310 K by using a digital temperature controller, Model 3700 (Scientific Instruments). The magnetic susceptibilities were calibrated by the use of $HgCo(NCS)_4$ and corrected for the diamagnetism of the ligands and anions, and the effective magnetic moments were calculated by the formula $\mu_{eff} = 2.83(\chi_M T)^{1/2}$, χ_M being a corrected molar magnetic susceptibility and T a temperature in K.

Mössbauer spectroscopy was effected by using a constant-acceleration spectrometer (Austin Science Associates (ASA)). Data were stored in a 1024-channel pulse height analyzer, Type 5200 (Inotech, Inc.). The temperature was monitored with a calibrated copper vs. constantan thermocouple within a variable-temperature cryostat, Type ASAD-4V-(ASA). A cobalt-57 source of 10 mCi diffused into a palladium foil was used for the absorption measurement. Some of the spectra were fitted to the Lorentzian line shape by using a least-squares method at the Computer Center, Kyushu University. Isomer shifts are reported with respect to the centroid of the spectrum of an iron foil enriched with ^{57}Fe.

The instrumental arrangement used for the EDD experiment is as follows. A rotating Au anode was used as the target of a white X-ray beam. X-ray beams were about 1 mm in diameter on the surface of samples. The data were taken in transmission. The energy region of the X-ray beams used was approximately 3–30 keV. A rotating-anode generator was operated at 35 kV–50 mA. The experiments were done at a fixed Bragg angle of $2\theta = 20°$. Photons diffracted from samples are detected with a solid-state detector (SSD), of which an energy resolution is 150 eV at 5.8 keV. The distance between a sample and the detector is about 150 mm. The SSD can be moved in the horizontal or vertical plane to within $^1/_{100}°$. Signals from the SSD are transformed both by a preamplifier and a main amplifier and are converted by an analog–digital converter (ADC). A multichannel analyzer (MCA) with 4K memory resolves the energy spectrum E_j of digital signals from ADC and stores the spectrum. Samples are set in a cryostat and the temperature is adjusted within ±0.1 °C at each temperature.

X-ray Crystal Structure Analysis

A crystal with dimensions of 0.3 × 0.2 × 0.5 mm was used for the X-ray analysis. Unit cell parameters and intensities were measured on a Rigaku AFC-5 automated four-circle diffractometer with graphite-monochromated Mo Kα radiations (λ = 0.71069 Å) at 19 ± 1 °C. Accurate cell dimensions were determined by least-squares calculations with 2θ values of 15 high-angle reflections. Intensity data were collected by the θ–2θ scan technique with a scan rate of 4° (2θ) min^{-1}. For weak reflections the peak scan was repeated up to four times, depending on their intensities. Three standard reflections were monitored after every 100 reflections, and their intensities showed a good stability. The intensity data were corrected for Lorentz and polarization effects, but not for absorption. A total of 3163 reflections with $2.5° \le 2\theta \le 54°$ were collected, of which independent 2426 reflections had $|F_o| \ge 3\sigma(|F_o|)$ and were employed in the solution and refinement of the structure.

Determination of structural parameters was carried out by direct methods by using a local version of the Universal Crystallographic Computation Program System UNICS III (MULTAN)[13] and the Ortep program on a FACOM 380S Computer at the Computer Center, Kyushu University. Atomic scattering factors for non-hydrogen atoms were taken from ref 14, and those for hydrogen atoms were taken from Stewart et al.[15] The four fluorine atoms in the PF_6^- ion were subjected to a disorder assuming a rotation about one F–P–F axis. All the hydrogen atoms were found on a difference Fourier map and included in further refinement with isotropic thermal parameters. Reliability factors are defined as $R = \sum||F_o| - |F_c||/\sum|F_o|$ and $R_w = [\sum w(|F_o| - |F_c|)^2/\sum w|F_o|^2]^{1/2}$, where the weighting schemes were taken as $w = [\sigma_c^2 + (0.015|F_o|)^2]^{-1}$. The final values of R and R_w were 3.87 and 5.85, respectively. The values of μ = 7.28 cm^{-1}, $F(000)$ = 594, and fw = 579.04 are estimated. Final positional and thermal parameters with their estimated standard deviations are given in Table I. Since the complex cation is well-defined and the PF_6^- ion was not of primary interest, this disorder problem was not pursued further.

Table I. Positional Parameters for $[Fe(acpa)_2]PF_6$[a]

atom	x/a	y/b	z/c
Fe	0.7500 (0)	0.4822 (1)	0.5000 (0)
P	0.7500 (0)	1.0881 (2)	0.0000 (0)
O	0.8406 (2)	0.6151 (3)	0.6212 (3)
N1	0.6392 (2)	0.3241 (3)	0.4083 (3)
N2	0.6695 (2)	0.4660 (3)	0.6373 (3)
C1	0.6266 (3)	0.2639 (4)	0.2865 (4)
C2	0.5508 (4)	0.1682 (5)	0.2305 (5)
C3	0.4853 (4)	0.1319 (5)	0.3009 (6)
C4	0.4986 (3)	0.1932 (5)	0.4250 (5)
C5	0.5758 (3)	0.2891 (4)	0.4765 (4)
C6	0.5927 (3)	0.3579 (4)	0.6115 (4)
C7	0.6813 (3)	0.5461 (4)	0.7434 (4)
C8	0.7539 (3)	0.6535 (4)	0.7799 (4)
C9	0.8272 (3)	0.6827 (4)	0.7228 (4)
C10	0.6165 (4)	0.5245 (5)	0.8349 (5)
C11	0.9025 (5)	0.7995 (6)	0.7755 (7)
F1	0.7500 (0)	1.2369 (6)	0.0000 (0)
F1′	0.7500 (0)	0.9344 (6)	0.0000 (0)
F2	0.7776 (3)	1.0873 (4)	0.1623 (3)
F3	0.6345 (3)	1.0844 (10)	−0.0252 (5)
H(C1)	0.6714 (0)	0.3068 (0)	0.2292 (0)
H(C2)	0.5424 (0)	0.1265 (0)	0.1464 (0)
H(C3)	0.4357 (0)	0.0558 (0)	0.2718 (0)
H(C4)	0.4430 (0)	0.1746 (0)	0.4691 (1)
H1(C6)	0.5309 (0)	0.3865 (0)	0.6224 (1)
H2(C6)	0.6160 (0)	0.2829 (0)	0.6840 (1)
H(C8)	0.7558 (0)	0.7063 (1)	0.8628 (1)
H1(C10)	0.5431 (0)	0.5200 (0)	0.7792 (1)
H2(C10)	0.6371 (0)	0.4403 (0)	0.8798 (1)
H1(C11)	0.8875 (0)	0.8479 (0)	0.6899 (1)
H2(C11)	0.9751 (0)	0.7764 (0)	0.8075 (1)
H3(C10)	0.6330 (0)	0.6036 (0)	0.9034 (1)
H3(C11)	0.8800 (0)	0.8651 (0)	0.8273 (1)

[a] Estimated standard deviations for the last significant figure are given in parentheses.

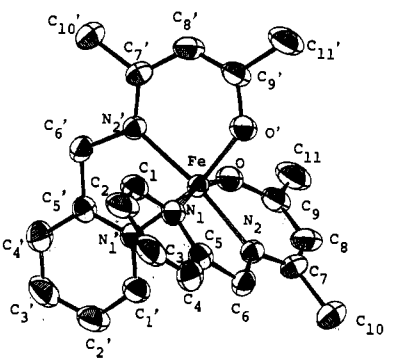

Figure 1. Perspective drawing of the $[Fe(acpa)_2]^+$ cation in $[Fe(acpa)_2]PF_6$.

(12) Hidaka, M.; Fujii, H.; Garrard, B. J.; Wanklyn, B. M. *Phys. Status Solidi A* **1984**, *86*, 75.

(13) Sakurai, T.; Kobayashi, K. *Rikagaku Kenkyusho Hokoku*, **1979**, *55*, 69; Kawano, S. *Rep. Comput. Cent., Kyushu* Univ. **1980**, *13*, 39.

(14) *International Tables for X-ray Crystallography*; Kynoch: Birmingham, England, 1974; Vol. IV.

(15) Stewart, R. F.; Davidson, E. R.; Simpson, W. T. *Chem. Phys.* **1965**, *42*, 3175.

Table II. Bond Lengths (Å) for $[Fe(acpa)_2]PF_6$[a]

Fe–O	1.939 (2)	Fe–N1	2.153 (2)
Fe–N2	2.081 (2)	N1–C1	1.356 (4)
C1–C2	1.370 (4)	C2–C3	1.383 (5)
C3–C4	1.374 (5)	C4–C5	1.384 (4)
C5–N1	1.339 (3)	C5–C6	1.496 (4)
N2–C6	1.457 (3)	N2–C7	1.319 (3)
C7–C10	1.511 (4)	C7–C8	1.415 (4)
C8–C9	1.364 (4)	C9–C11	1.505 (6)
C9–O	1.297 (4)	C1–H(C1)	0.970 (3)
C2–H(C2)	0.838 (3)	C3–H(C3)	0.886 (4)
C4–H(C4)	0.966 (3)	C6–HA(C6)	0.993 (3)
C6–HB(C6)	1.000 (3)	C8–H(C8)	0.895 (3)
C10–HA(C10)	0.913 (3)	C10–HB(C10)	0.955 (4)
C10–HC(C10)	0.920 (4)	C11–HA(C11)	0.854 (4)
C11–HB(C11)	0.971 (5)	C11–HC(C11)	0.928 (5)
P–F1	1.586 (3)	P–F2	1.523 (15)
P–F3	1.614 (6)	P–F4	1.647 (5)
P–F5	1.475 (7)		

[a] Estimated standard deviations for the last significant figure are given in parentheses.

Table III. Bond Angles (deg) for $[Fe(acpa)_2]PF_6$[a]

Fe–N1–C5	116.3 (1)	Fe–N1–C1	124.9 (2)
O–Fe–N1	166.0 (1)	O–Fe–N2	89.0 (1)
N1–Fe–N2	77.5 (1)	O–Fe–O′	94.3 (1)
O–Fe–N2′	97.0 (1)	O–Fe–N1′	91.0 (1)
N1–Fe–O′	91.0 (1)	N1–Fe–N2′	95.9 (1)
N1–Fe–N1′	86.7 (1)	N2–Fe–O′	97.0 (1)
N2–Fe–N2′	171.2 (1)	N2–Fe–N1′	95.9 (1)
N1′–Fe–N2′	77.5 (1)	N1′–Fe–O′	166.0 (1)
N2′–Fe–O′	89.0 (1)	N1–C1–C2	122.1 (3)
C1–C2–C3	118.9 (3)	C3–C4–C5	119.3 (3)
C4–C5–N1	121.8 (3)	C5–N1–C1	118.7 (2)
N1–C5–C6	117.1 (2)	C5–C6–N2	111.6 (2)
C6–N2–Fe	117.1 (2)	C6–N2–C7	117.5 (2)
N2–C7–C8	122.8 (3)	C7–C8–C9	127.1 (3)
C8–C9–O	124.4 (2)	C9–O–Fe	129.4 (2)
N2–C7–C10	120.3 (2)	C10–C7–C8	116.9 (2)
C8–C9–C11	120.5 (3)	C11–C9–O	115.2 (3)
C4–C5–C6	121.2 (3)		

[a] Estimated standard deviations for the last significant figure are given in parentheses.

Results and Discussion

Crystal and Molecular Structure of $[Fe(acpa)_2]PF_6$. A perspective drawing of the $[Fe(acpa)_2]^+$ cation and the numbering system are illustrated in Figure 1. The bond lengths and angles are summarized in Tables II and III. The environment of the cation is comprised of N_4O_2 donors of acpa moieties and a pseudooctahedral coordination with cis geometry for the two oxygen atoms. The two ligands are related by a crystallographic 2-fold axis. The Fe–O bond distance associated with the acetylacetone residue is the shortest (1.939 Å). The Fe–N1 bond length associated with pyridine is longer than the Fe–N2 bond associated with amine. The average iron–donor atom distance is 2.058 Å and is in accordance with the values reported for other high-spin iron(III) complexes with N_4O_2 donors. It is well known that the average iron–donor atom distances in high-spin complexes are longer by 0.13 Å than those in low-spin complexes.[16-18] The angles O–Fe–N1 and N2–Fe–N2′ deviate markedly from 180° for an ideal octahedron (166° and 171° respectively).

Magnetic Susceptibilities. The temperature dependences of the magnetic susceptibilities and the area under the Mössbauer resonance curve for $[Fe(acpa)_2]PF_6$ are shown in Figure 2. The continuous transition of high spin ⇌ low spin was observed in accordance with the data reported earlier. The magnetic moments are 5.85 μ_B at 303 K and 2.00 μ_B at 80 K. Any hysteresis effect was not observed within experimental errors, and completeness of the transition at both high- and low-temperature limits is observed in accordance with the Mössbauer measurements. The half-transition temperature is estimated to be 187 K, assuming simple additive properties in magnetic susceptibilities $\mu^2 = x\mu_h^2 + (1 - x)\mu_l^2$, where x is the fraction of high-spin isomers. The magnetic susceptibilities of ^{57}Fe-enriched $[^{57}Fe(acpa)_2]PF_6$ showed temperature profiles similar to the those of unenriched samples.

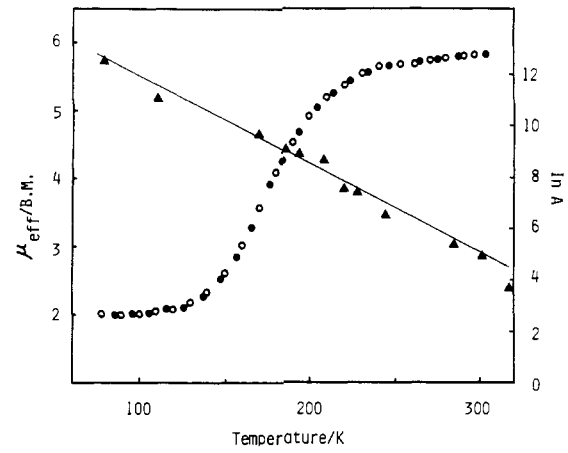

Figure 2. Temperature dependences of the magnetic moments O for decreasing temperature, ● for increasing temperature and ln A (▲) for $[Fe(acpa)_2]PF_6$.

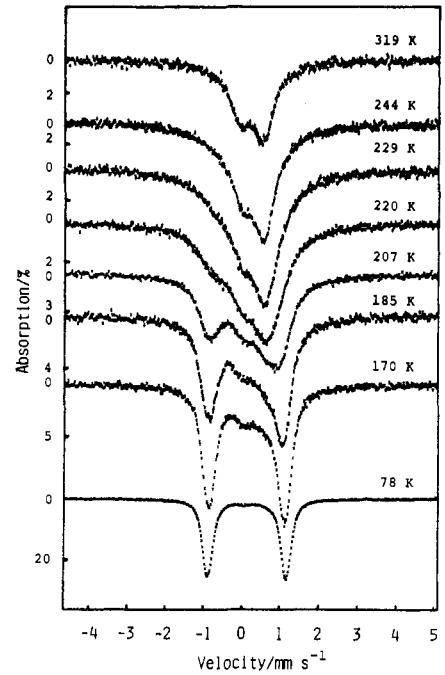

Figure 3. Representative Mössbauer spectra for $[^{57}Fe(acpa)_2]PF_6$ at various temperatures.

Mössbauer Spectra. The ^{57}Fe-enriched $[^{57}Fe(acpa)_2]PF_6$ was prepared to determine the exact spin-interconversion rate of the complexes, and the Mössbauer spectra were measured at various temperatures (Figure 3). The temperature dependence of the relative area under the Mössbauer resonance curve is plotted in Figure 2. The plotting follows a curve rather than a straight line due to the difference of the recoilless fraction between high-spin and low-spin isomers. Analysis of the spectra on the basis of two pairs of doublets consisting of both high-spin and low-spin isomers was inadequate because the spectra show electronic relaxation between high-spin and low-spin states. If the spectra are analyzed as a single doublet, the spectra may have a quadrupole splitting (QS) of 2.235 mm/s and an isomer shift (IS) of 0.245 mm/s at

(16) Sinn, E.; Sim, G.; Dose, E. V.; Tweedle, M. F.; Wilson, L. J. *J. Am. Chem. Soc.* **1978**, *100*, 3375.
(17) Leipoldt, J. G.; Coppens, P. *Inorg. Chem.* **1973**, *12*, 2269.
(18) Matsumoto, N.; Ohta, S.; Yoshimura, C.; Ohyoshi, A.; Kohata, S.; Okawa, H.; Maeda, Y. *J. Chem. Soc., Dalton Trans.* **1985**, 2575.

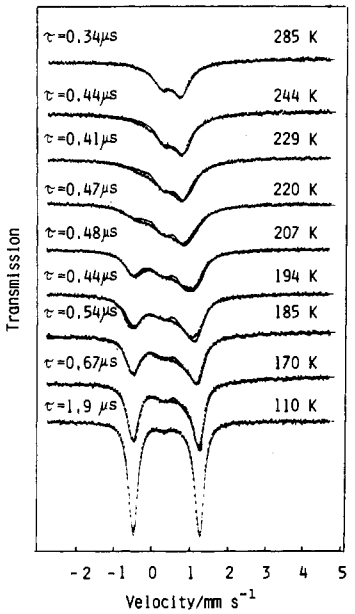

Figure 4. Attempt to obtain a best fit between the Mössbauer spectra for [^{57}Fe(acpa)$_2$]PF$_6$ and the model by using the correlation times described in the figure.

78 K and QS of 0.529 mm/s and IS of 0.330 mm/s at 319 K. The large quadrupole splitting at 78 K seems to be due to the unsymmetrical nature of the ligand, i.e. the distortion created by the tridentate coordination of the ligands at the site of an iron atom. The cis geometry for the two oxygen atoms brings about QS values twice as large as the trans value.[19] This geometry is in accordance with the ESR result that the unpaired electron resides in the d_{xy} orbital in the octahedral approximation.[6]

The simulation of the Mössbauer spectra was carried out in order to measure directly the spin-interconversion rate constants and/or spin-state lifetimes in the solid state. The theoretical Mössbauer spectra is calculated from eq 1,[20] in which the subscript

$$I(\omega) = \sum_i K'\{(1 + \tau\Gamma)P_i + Q_iR_i/(P_i^2 + R_i^2)\} \qquad (1)$$

i refers to an individual Mössbauer transition and where $P_i = \tau[\Gamma^2 - \{^1/_2(\omega_i^h + \omega_i^l) - \omega\}^2 + {}^1/_4(\omega_i^h - \omega_i^l)^2] + \Gamma$, $Q_i = \tau\{^1/_2(\omega_i^h + \omega_i^l) - \omega - {}^1/_2(p_h - p_l)(\omega_i^h - \omega_i^l)\}$, and $R_i = \{^1/_2(\omega_i^h + \omega_i^l)(1 + 2\tau\Gamma) + {}^1/_2(p_h - p_l)(\omega_i^h - \omega_i^l)\}$. The constant K' is the relative intensity of the ith transition, and p_h and p_l are the populations of high-spin and low-spin isomers, respectively. In our model the relaxation process occurs between the high-spin and low-spin energy levels. In the fitting of the experimental spectra to this model, the values of isomer shift at both isomers were varied with temperature by assuming a second-order Doppler shift of 5×10^{-4} mm/(s K). Although line widths are important to analyze relaxation spectra, line widths were varied in proportion to the population of the high-spin isomer within the range from $\Gamma = 0.41$ to 0.66 mm/s because the full-width at half-maximum of the high-spin isomer ($\Gamma = 0.75$ mm/s at 319 K) is larger than that of the low-spin isomer ($\Gamma = 0.36$ mm/s at 78 K). Asymmetry of line intensity and populations of high-spin or low-spin isomers were parameterized as well as relaxation times. The populations of the high-spin isomers obtained in this simulation are 10% smaller than those calculated from the magnetic susceptibility data.

The computer minimizations of eq 1 resulted in the theoretical spectra presented in Figure 4. The fit is not so good at around 200 K because the increase of the population of $^6A_{1g}$ state makes the line width broad due to spin–spin relaxation and/or spin–lattice relaxation. Furthermore the temperature dependence of the quadrupole splitting of low-spin isomers is not taken into consideration. Therefore, the calculated relaxation times may be convincing only at low temperatures. The analysis is based on assumptions concerning the relationship of the axis of quantization in the low-spin and high-spin species. The EDD results described later suggest no crystallographic phase transition in the spin-transition region. The quadrupole splitting decreases linearly with rising temperature. The above observation may suggest that the axis of quantization of one isomer is nearly coaxial with that of the other isomer.[18] The lifetimes of the low-spin and high-spin states are shown by τ_l and τ_h, respectively. The observed correlation times ($\tau = \tau_l\tau_h/(\tau_l + \tau_h)$) span a range from 1.9×10^{-6} to 0.34×10^{-6} s and are dependent on temperature. The rates for the forward k_1 and reverse k_{-1} rate constants for the spin interconversion $^2T_{2g} \rightleftharpoons {}^6A_{1g}$ are defined as $1/\tau_l$ and $1/\tau_h$, respectively. The equilibrium constant $K = k_1/k_{-1}$ was found to be temperature-dependent, thus the transition mechanism will not be simple in the thermodynamic aspect.

The spectral shape of [Fe(acpa)$_2$]PF$_6$ taken at 230 K is very similar to the spectrum at 229 K for [^{57}Fe(acpa)$_2$]PF$_6$. The complex [Fe(acpa)$_2$]PF$_6$ is not so sensitive to the preparation method although spin-crossover complexes are often sensitive to the preparation method or the solvent used for crystallization.

Energy-Dispersive X-ray Diffraction. Energy-dispersive X-ray diffraction patterns have been recorded for [Fe(acpa)$_2$]PF$_6$ at various temperatures. Figure 5 shows a representative spectrum of (0n0) reflections for a single crystal of [Fe(acpa)$_2$]PF$_6$. In the figure, the ordinate is the number of photons per channel and the abscissa is the channel number, which can be transformed to energy by E (keV) = 0.0300 × (channel number). Reflections indexes observed are shown in the figure. The temperature dependences of integral intensities of (030) and (050) reflections with strong intensities are shown in Figure 6, in which the integral intensities change continuously in the temperature range from 140 to 230 K in accordance with the temperature region of spin transition for the complexes. In the figure, the data of the (011)

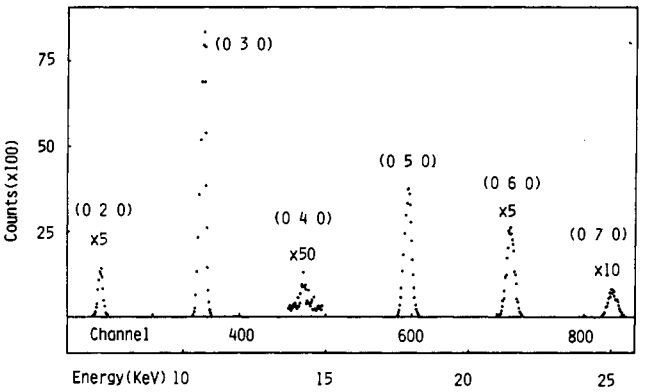

Figure 5. Representative spectrum of (0n0) reflections for a single crystal of [Fe(acpa)$_2$]PF$_6$.

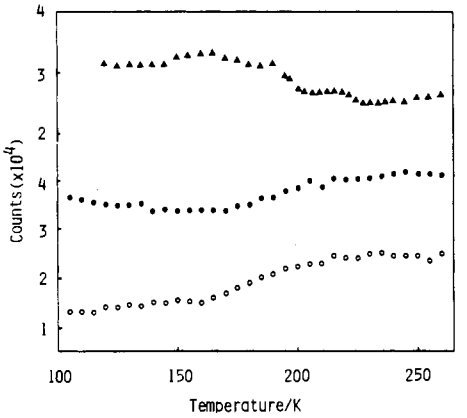

Figure 6. Temperature dependences of the partial integral intensities of the (030) (●) and the (050) (○) reflections for a single crystal and the (011) (▲) reflection for powdered crystals of [Fe(acpa)$_2$]PF$_6$.

(19) Gibb, T. C. *Principles of Mössbauer Spectroscopy*; Chapman and Hall: London, 1976.
(20) Wickman, H. H. *Mössbauer Effect Methodology*; Cruverman, I. J., Ed.; Plenum: New York, 1966; Vol. 2.

reflection for the powdered complexes are also plotted. The intensities for (011) reflections show complicated changes. The relative accuracy of the values is sufficient to establish this result. It is clear that there is no large difference in the structure between high-spin and low-spin states. In addition, the observations are good enough to rule out the possibilities of any crystallographic phase transition associated with a spin transition. The intensity modulation as shown in the figure can be related to the microstructural changes of individual molecules and/or production of clusters of constituent molecules either statically or dynamically. It is, therefore, possible to expect a random distribution of two spin isomers; modulation of the molecular array and the reorderings of the molecular array and/or atomic arrays through the spin transition take place dynamically without a significant domain formation by either of the two spin isomers. In tris(dithiocarbamato)iron(III), which exhibits rapid electronic relaxation, the two spin isomers were not crystallographically resolved and only an average structure was reported.[17]

The mechanism of a continuous spin transition in a solid state and the factors that determine electron-transfer rates are not yet understood although it is pointed out that a coupling between the electronic state and the vibrational modes of a molecule is important for spin transition in solution.[21] In the system studied here, no evidence of first-order transition could be found. It may be important to image a intramolecular mechanism for rapid spin interconversion.

Registry No. Hacpa, 28484-27-7; $[Fe(acpa)_2]PF_6$, 90790-59-3; acetylacetone, 123-54-6; 2-(aminomethyl)pyridine, 3731-51-9.

Supplementary Material Available: Listings of programming data, thermal parameters, and mean-square displacement tensors of atoms (5 pages). Ordering information is given on any current masthead page.

(21) Sutin, N. *Acc. Chem. Res.* **1982**, *15*, 275.

Contribution from the Departament de Química Inorgànica, Facultat de Química, and Departament de Cristal.lografia, Facultat de Geologia, Universitat de Barcelona, Diagonal 647, 08028 Barcelona, Spain

Structure–NMR Correlations in Halo(ligand)bis(dioximato)cobalt(III) Complexes

Concepción López,[†] Santiago Alvarez,*[†] Xavier Solans,[‡] and Manuel Font-Altaba[‡]

Received December 6, 1985

A synthetic scheme leading to chloro(ligand)bis(dimethylglyoximato)- and chloro(ligand)bis(diphenylglyoximato)cobalt(III) complexes in good yields is reported for the cases where the ligand is a nitrogenated aromatic base. Substitution reactions of the axial chloro ligand lead to the cyano ligand derivatives. Single-crystal X-ray diffraction and NMR spectroscopic studies were carried out to characterize the above-mentioned complexes. Crystal structures of the following compounds are reported: $[Co(dmgH)Cl(4\text{-}NCpy)]\cdot{}^1/_3H_2O$ (**1**), $[Co(dmgH)_2X(2,6\text{-}Me_2pz)]$ (X = Cl (**3**) and Br (**13**)), and $[Co(dmgH)_2Cl(3,5\text{-}Me_2pzol)]$ (**5**), where dmgH = dimethylglyoximate(1−), 4-NCpy = 4-cyanopyridine, $2,6\text{-}Me_2pz$ = 2,6-dimethylpyrazine, $2,6\text{-}Cl_2pz$ = 2,6-dichloropyrazine, and $3,5\text{-}Me_2pzol$ = 3,5-dimethylpyrazole. Compound **1** is orthorhombic, space group $P2_12_12_1$, with $Z = 4$ and unit cell parameters $a = 15.690$ (3) Å, $b = 14.367$ (3) Å, and $c = 8.320$ (2) Å. Compound **3** is monoclinic, space group $P2_1/a$, with $Z = 4$ and unit cell parameters $a = 12.827$ (2) Å, $b = 16.836$ (3) Å, $c = 8.667$ (1) Å, and $\beta = 99.10$ (2)°. Compound **5** is monoclinic, space group $P2_1/a$, with $Z = 4$ and unit cell parameters $a = 16.139$ (3) Å, $b = 13.525$ (1) Å, $c = 8.491$ (1) Å, and $\beta = 103.94$ (2)°. Compound **13** is monoclinic, space group $P2_1/a$, with $Z = 4$ and unit cell parameters $a = 13.019$ (2) Å, $b = 16.816$ (3) Å, $c = 8.827$ (1) Å, and $\beta = 98.84$ (2)°. ^1H and ^{13}C NMR chemical shifts of the organic bases show clear correlations with both the position of the atoms relative to the bis(dioximato)cobalt moiety and the wavelength of the Co → dmgH charge-transfer band; these correlations can be rationalized with the aid of the ring-current formalism usually associated with organic aromatic molecules.

The chemistry and molecular structure of bis(dioximato)cobalt(III) complexes (hereafter referred to by the generic name of cobaloximes) have been extensively explored in the last few years[1] due to interest in them as models for important biochemical complexes[2] as well as to their usefulness as catalysts in many chemical processes[3] or as templates in many organic syntheses.[4] In this context, the knowledge of the electronic structure of cobaloximes and the understanding of the related cis and trans influences is sought as a cornerstone for a systematization of the large body of chemical information currently available and for the successful design of novel derivatives with desired properties.

The study of structure–properties relationships might provide a hint toward the understanding of these problems. Several workers[5-7] have investigated ^1H NMR spectra of cobaloximes in order to establish cis and trans influences of X and L ligands in $[Co(dioxH)_2X(L)]$ complexes (dioxH = dioximate(1−) ligand) and found some correlations between the resonance of methylic protons of the $Co(dmgH)_2^+$ moiety and the ligand field parameter[6] or the pK_a of the axial L group.[7]

On the other hand, only a few studies on the ^{13}C NMR spectra of cobaloxime derivatives have been previously reported.[5a,8] Attempts to correlate ^1H and ^{13}C resonances were made, but the results were rather poor. A thorough study on ^{31}P NMR spectra and structural data of mixed phosphine–cobaloxime complexes has also been reported.[8,9]

[†] Departament de Química Inorgànica, Facultat de Química.
[‡] Departament de Cristal.lografia, Facultat de Geologia.

(1) (a) Bresciani-Pahor, N.; Forcolin, M.; Marzilli, L. G.; Randaccio, L.; Summers, M. F.; Toscano, P. J. *Coord. Chem. Rev.* **1985**, *63*, 1. (b) Toscano, P. J.; Marzilli, L. G. *Prog. Inorg. Chem.* **1984**, *31*, 105. (c) Samus, N. M.; Ablov, A. V. *Coord. Chem. Rev.* **1979**, *28*, 177. (d) Chakravorty, A. *Coord. Chem. Rev.* **1974**, *13*, 1.
(2) (a) Schrauzer, G. N.; Kohnle, J. *Chem. Ber.* **1964**, *97*, 3056. (b) Schrauzer, G. N. *Acc. Chem. Res.* **1968**, *1*, 97. (c) B_{12}; Dolphin, D., Ed.; Wiley-Interscience: New York, 1982; Vol. 1 and 2.
(3) (a) Rockenbauer, A.; Eyor, M.; Kwiecinski, M.; Tyrlik, S. *Inorg. Chim. Acta* **1982**, *58*, 237. (b) Noguchi, M.; Kambara, S. *J. Polym. Sci., Part B* **1963**, 553. (c) Nemeth, S.; Simandi, L. *J. Mol. Catal.* **1982**, *14*, 87.
(4) *Houben-Weyl Methoden der Organischen Chemie*, 4th ed., Langer, E., Ed.; Thieme: Stuttgart, West Germany, 1984; Vol. 13/9b, Metallorganische Verbindungen, pp 1–284.
(5) (a) Stewart, R. G.; Marzilli, L. G. *Inorg. Chem.* **1977**, *16*, 924. (b) Trogler, W. C.; Marzilli, L. G. *Inorg. Chem.* **1975**, *14*, 2942. (c) Trogler, W. C.; Stewart, R. C.; Epps, L. A.; Marzilli, L. G. *Inorg. Chem.* **1974**, *13*, 1564.
(6) Hill, O. A.; Morallee, K. G. *J. Chem. Soc. A* **1969**, 554.
(7) Bied-Charreton, C.; Alain, L.; Gaudemer, A. *Bull. Soc. Chim. Fr.* **1972**, 861.
(8) Kargol, J. A.; Crecely, R. W.; Burmeister, J. L.; Toscano, P. J.; Marzilli, L. G. *Inorg. Chim. Acta* **1980**, *40*, 79.
(9) Marzilli, L. G.; Toscano, P. J.; Ramsden, J. H.; Randaccio, L.; Bresciani-Pahor, N. *Catalytic Aspects of Metal Phosphine Complexes*; Advances in Chemistry 196; American Chemical Society: Washington, DC, 1982; p 85.

0020-1669/86/1325-2962$01.50/0